Proceedings World Geothermal Congress 2020+1
Reykjavik, Iceland, April - October 2021

3D Static Modeling Update of the Salak Geothermal Field, Indonesia: Earth Science-Defined Conceptual Features and Reservoir Properties for the New Numerical Model

Nur Vita Aprilina[1], Fanji Junanda Putra[1], Glenn U. Golla[1], Gregg Nordquist[2]

[1]Star Energy Geothermal Salak, Sentral Senayan II Office Tower 25th Floor, Jalan Asia Afrika No. 8, Jakarta 10270, Indonesia

[2]Independent Consultant

nvaprilina@starenergy.co.id

Keywords: Salak, fracture permeability, fracture spacing, Petrophysical Group (PG), Effective Fractures (EF)

ABSTRACT

In 2017, the Salak 3D Modeling Team completed an update of the Salak 3D Static Model that will be the basis for providing earth science-defined conceptual features and reservoir properties for the new Numerical Model of the Salak Geothermal Field. The updated 3D Static Model incorporates Best Practices for interpreting and distributing matrix porosity (Φ_{matrix}) and permeability (k_{matrix}) and defining the top and base of the reservoir (ToR and BoR). Also incorporated into the updated 3D Static Model data-driven basis for defining the grid orientation, and the interpretation and fieldwide distribution of fracture permeability, permeability anisotropy, and fracture spacing.

The updated 3D Static Model uses a different approach to define the distribution of matrix porosity and permeability properties than used previously at Salak. While the previous Static Model used a kriging approach, the updated Static Model includes formations that were divided into Petrophysical Groups (PG) and porosity and permeability measurements from cores for each PG were averaged. In addition, instead of the low, medium, and high cases for ToR and BoR, previoulsy used, the updated 3D Static Model uses a concept-driven approach for the distribution of commercial and connected fractures. These new criteria were modified to describe the fracture system in the geothermal naturally fractured reservoir that has areas of connected but lower permeability at the reservoir margins and commercial, higher permeability area at the core of the reservoir. For the first time, the orientation of the simulation grid for the numerical model is based on the dominant trend of the Effective Fractures (EFs), or fractures that produce geothermal fluids, as determined from borehole image logs. This provides a quantitative basis for defining the dominant permeability anisotropy in the model. Lastly, 3D distribution of fracture permeability and fracture spacing were included in the updated 3D Static Model, and were not in the previous Static Model.

The next step involves a collaborative review and update of the parameters for the new Salak Numerical Model during the initial state and history matching phases by a joint Earth Science (ES) and Reservoir Engineering (RE) team. This is key to reviewing the effectiveness of the new Best Practices for defining ES-based constraints for the Numerical Model. As additional lessons are learned, these Best Practices will be reviewed and modified, as needed.

1. INTRODUCTION

The Salak geothermal field is located in West Java, Indonesia along the Sunda Volcanic Arc (**Figure 1**). It is situated in a mountainous area with elevation ranging from about 950 to 1,500 m above sea level (ASL). The field is about 60 kilometers from Jakarta, capital city of Indonesia. Salak is a liquid-dominated geothermal system with a moderate- to high-temperature (464°-600°F) fracture-controlled hosting benign and low to moderate non-condensable gas (NCG) fluids (Stimac et al., 2008).

An update of the Salak 3D Static Model was completed in 2017 to integrate recent subsurface data, leverage the latest learnings from the recent update of the Darajat 3D Static Model, and incorporate new fracture characterization insights and workflows. The newly updated Static Model provides the most up-to-date Static Model for the new Simulation Model. This paper describes the updates on the Salak 3D Static Model including the ES inputs and constraints for the updated Salak Numerical Model. The steps needed in building updated Salak 3D Static Model are also described including new grid establishment, populating updated reservoir properties, and exporting the Static Model to Tecplot as an interface to the Simulation Model.

2. NEW GRID GENERATION

The stratigraphic grid built for the previous 3D Static Model was not oriented, used a finer grid size of 100 x 100 x 30 m, and had irregular shape as it followed the general surfaces of the different formations (**Figures 2** and **3**). To accommodate a requirement of and optimize time in Numerical Modeling, a new grid was generated for the 3D Static Model. The new grid has the x-axis with a N22°E orientation based on the observed dominant EF orientation. The histogram of dip azimuth of fractures inside the Salak reservoir shows a concentrated population of fractures with an average dip azimuth of 112° or a strike orientation of N22°E which is parallel with S_{Hmax} tectonic stress orientation of ~N24°E (**Figure 4** from Golla et al., 2015). The same correlation between EFs and S_{Hmax} is observed at the Darajat Field, West Java, Indonesia (Golla et al., 2015).

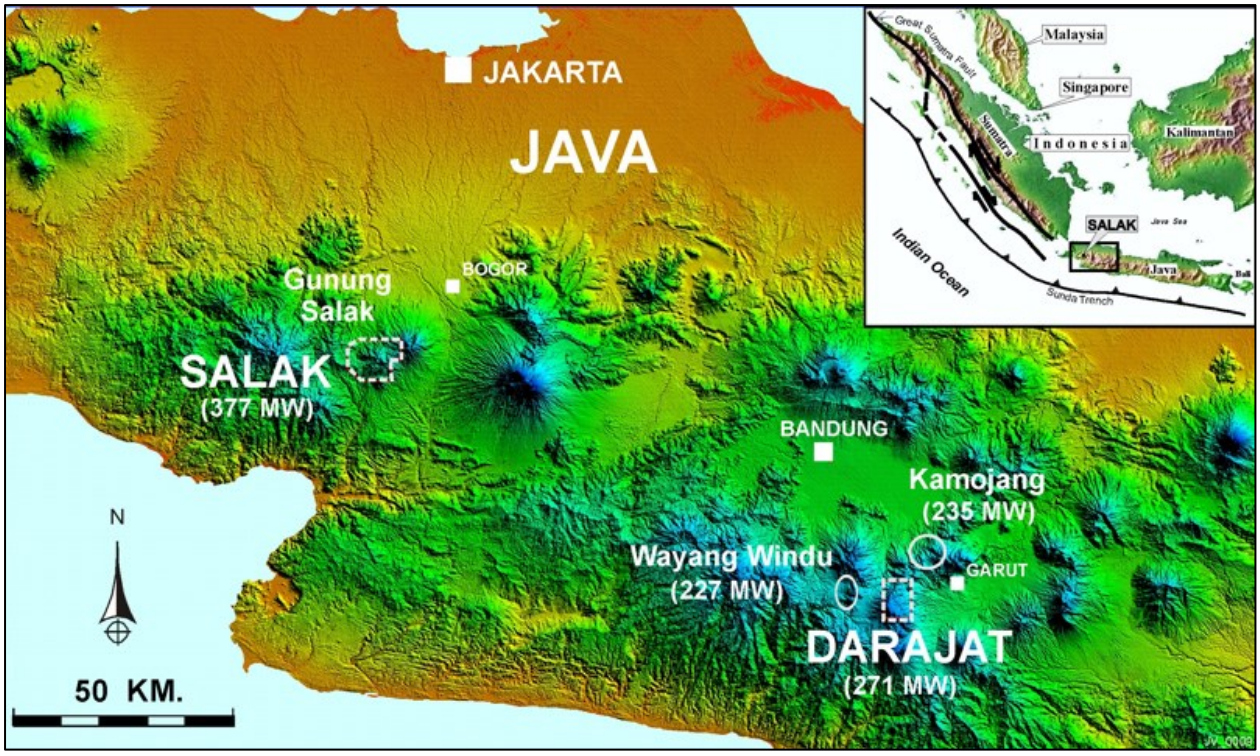

Figure 1: Map of West Java showing major cities and volcanic centers. Also shown are the Salak, Darajat, and Wayang Windu geothermal contract areas (dashed polygons) and other producing geothermal field in the general area.

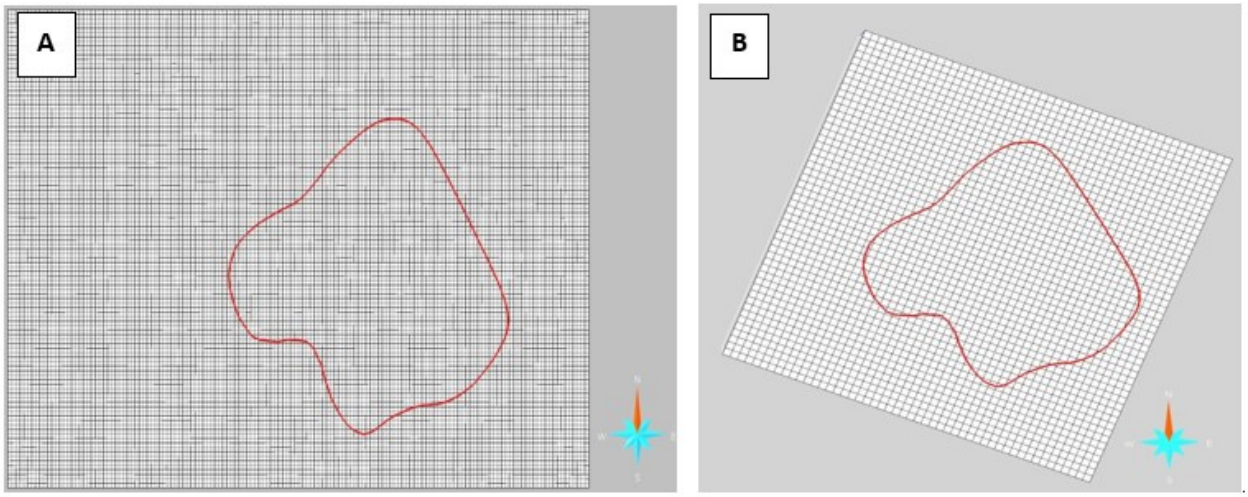

Figure 2: (A) Stratigraphic grid in the previous Salak 3D Static Model with north-south orientation. (B) New grid with N22°E orientation in the updated 3D Static Model.

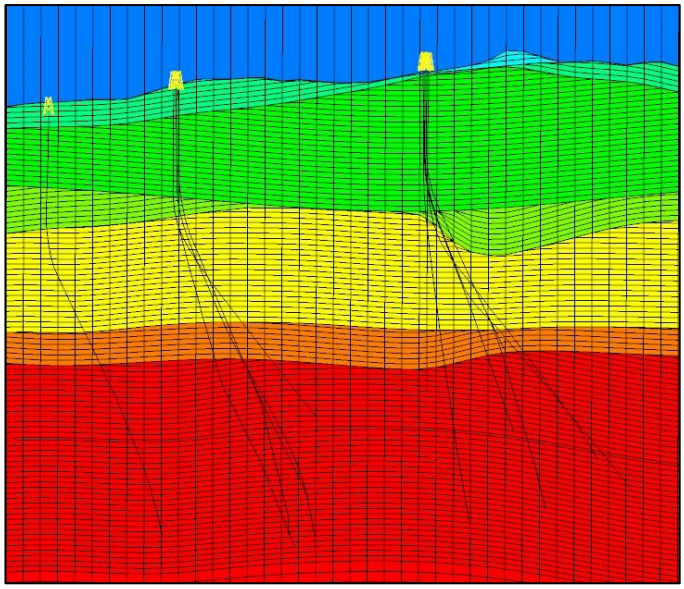

Figure 3: Cross-section along the previous 3D Static Model showing the irregular shape inside the reservoir which follows the formation surfaces.

The previous Static Model grid had an irregular shape following the formation surfaces (**Figure 3**). It was intended to make the grid honor the formation layers, especially the Rhyodacite Marker (RDM), an important formation in Salak. However, to allow efficiency during the simulation process, the new grid was established with regular sugar cube shape (**Figure 5**). Trial runs to test the grid were conducted using three kinds of grids with various sizes:

1. 200 x 200 x 200 m with finer vertical grid thickness of 100 m at 2,400 ft. ASL to 2,200 ft. BSL where the RDM and Middle Dacite Formations occur to allow more detailed observation of the liquid level;

2. 200 x 200 x 200 m with finer 100 x 100 x 100 m at the central part of the Salak field where there are more data from wells; and

3. 150 x 150 x 150 m, a slightly smaller size.

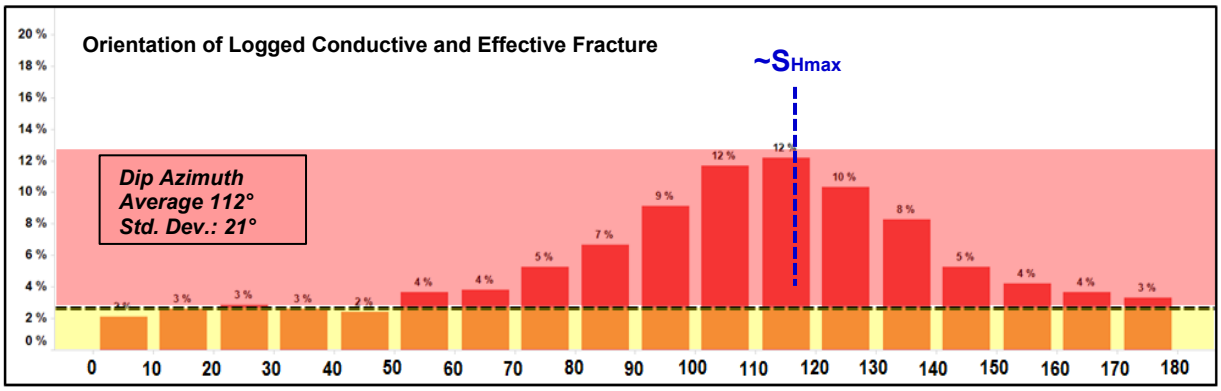

Figure 4: Histogram showing the distribution of dip magnitude of open fractures and EFs inside the Salak reservoir. The Y-axis denotes the percentage of fractures in one bin divided by all the data. The horizontal black dashed-line is the arbitrarily-picked boundary between the random/background and dominant sets of fractures.

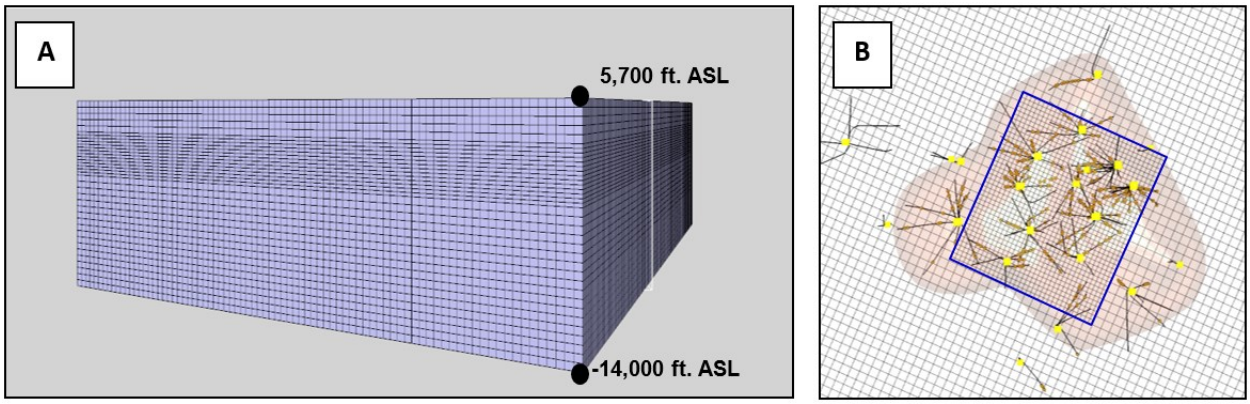

Figure 5: (A) 200m x 200m x 200m grid with finer vertical grid size of 100m at the interval where the RDM and Middle Dacite Formations were encountered. (B) The same 200m x 200m x 200m with a finer 100m x 100m x 100m grid at the central part of the Salak field.

A comparison of cell numbers in the three grids provided to the Numerical Modeling Engineers is summarized in **Table 1**. The number of cells in the 200 x 200 x 200 m-grid (with vertical finer grid of 100 m) is not significantly different with the number of cells in the current Numerical Model. Reservoir Engineering colleagues indicate that this grid seems to be efficient when run in Numerical Model; hence, the reservoir properties were transferred and redistributed in this grid. The 200 x 200 x 200 m-grid (with an interposed finer 100 x 100 x 100 m grid) provides a finer and more detailed scale in the Numerical Model (**Figure 6**). However, the exported grid from 3D Static Model was not tested in the Numerical Model and it is ambiguous if this grid can be run successfully in TOUGH2, the simulation software. In addition, the computing time to run this grid in Numerical Model is still uncertain.

Table 1: Comparison of the number of cells between the updated Salak 3D Static Model and current Numerical Model

Grid	Cell numbers
Current Numerical Model	7,605
Grid 200m x 200m x 200m with vertical finer grid of 100m at the Middle Dacite and RDM Formations	8,525* & 14,509**
Grid 200m x 200m x 200m with vertical & horizontal finer grid of 100m x 100m x 100m at the center part of Salak reservoir area	(+20,685)* & (+28,558)**
Grid 150m x 150m 150m	14,661* & 25,508**

Remarks: *cell numbers in commercial region **cell numbers in connected fracture region

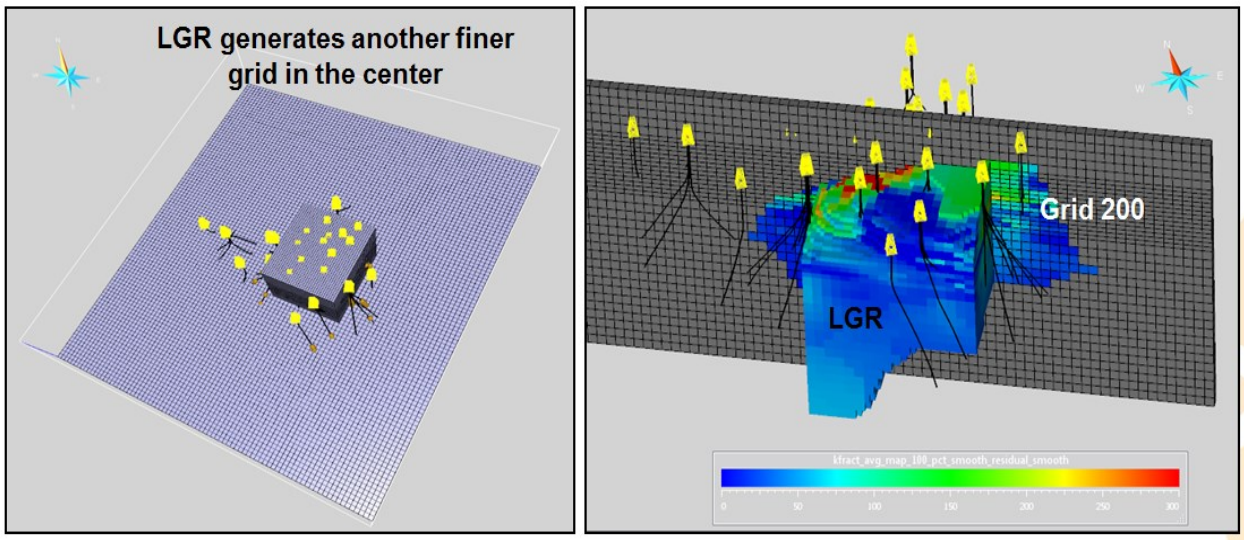

Figure 6: Grid with 200 x 200 x 200 m cells with finer 100 x 100 x 100 m subdivision at the central part of Salak field. These two interposing grids were generated with the Local Grid Refinement (LGR).

3. RESERVOIR DEFINITIONS

The updated Salak 3D Static Model used a different approach to establish reservoir definitions compared to what was applied in the previous 3D Static Model. Low, medium, and high cases of the ToR and BoR were previously used to provide the volume of reservoir to support estimates of reserves. In the updated Salak 3D Static Model, the criteria was modified to

emphasize our understanding of how reservoir processes may impact field performance rather than emphasizing the volumetric reserves representations. Also, this updated criteria is more appropriate as the steam cap develops in liquid dominated reservoir in East Salak. In the undrilled area, interpretation of reservoir boundary still uses the same criteria as applied in the previous model: clay cap distribution, distance from surface thermal manifestation (fumarole) locations, and extrapolated temperature distribution from adjacent wells (Aprilina et al., 2015).

3.1 Top of Reservoir (ToR)

The updated Salak 3D Static Model uses the following definitions to represent the ToR (Aprilina et al., 2016):

1. Top of Commercial Reservoir: represents the reservoir region with high, convective and isothermal temperature and location of permeable entries interpreted from PTS data.

2. Top of Connected Fracture Network: the region where the transition from conductive to convective temperature occurs and permeability is relatively low, but may still have a connection to outside aquifers for outflow and inflow of fluids.

The criteria used to define top of commercial region and connected fracture network is summarized in **Table 2.**

Table 2: Criteria used to define the tops of commercial and connected fracture network

Case	Criteria
Top of Commercial Reservoir	▪ First Pressure-Temperature-Spinner (PTS) permeable entry ▪ Top of isothermal/convective temperature profile ▪ Propylitic alteration – continuous epidote
Top of Connected Fracture Network	▪ Base of conductive temperature ▪ Propylitic alteration – first epidote

Compared to the description in the 2005 Salak Conceptual Model (Rohrs et al., 2005), the interpretation of top of the reservoir margins is similar but the updated Static Model has two new features. In addition to the traditional high temperature and convecting commercial resource, the new Static Model contains an outer envelope of lower permeability and lower temperature region. This outer envelope provides a more conceptually realistic interpretation of the reservoir margins, and allows for evaluation of edge field processes that could affect field performance, such as, condensation or gas accumulation at the top of the steam cap, entry of cooler marginal recharge, etc. Lastly, this outer region provides leeway to the Numerical Modeler to activate grid blocks, e.g., aquifers to explain cooling in certain wells, and obtain a reasonable history match.

The workflow used to generate the two ToR surfaces are similar with the workflow used in the previous Static Model where the well picks are used to hand-contour the ToR surfaces. However, in the previous model, the well picks of interpreted low, medium, and high cases of ToR were obtained from each well to generate ToR surfaces. In the updated Salak 3D Static Model, the ToR criteria (**Table 2**) were prioritized and strictly applied in defining the ToR, e.g., the top of the isothermal zone is the primary and start of continuous epidote is the last criterion used to define the commercial reservoir (**Figure 7**).

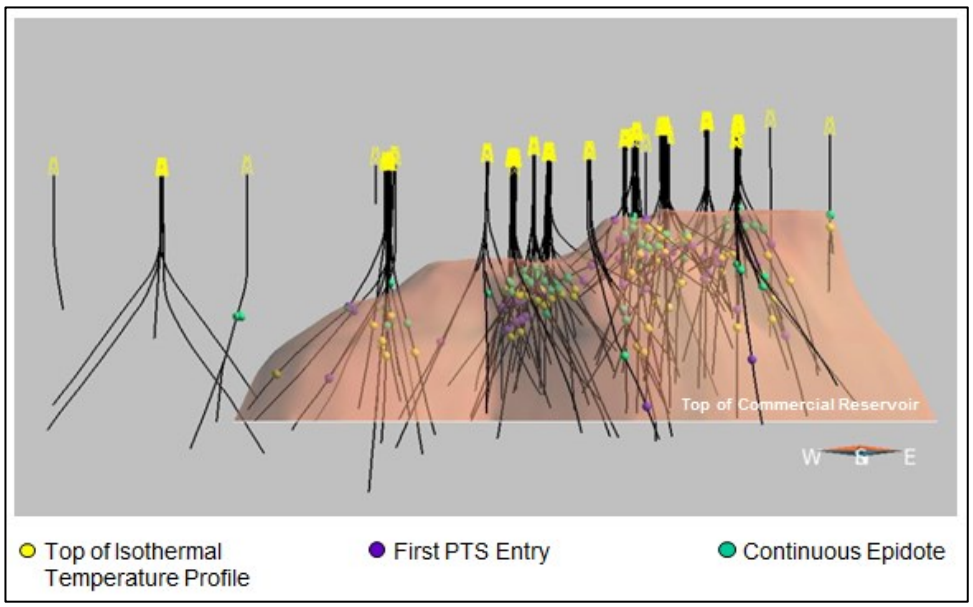

Figure 7: Well picks of each ToR criteria were defined to generate ToR surfaces.

Figure 8 shows the 3D representation of the Tops of Commercial Reservoir and Connected Fracture Network. In the central part of the field, the Tops of Commercial Reservoir and Connected Fracture Network are nearly coincident with each other. Near the margins (e.g., well 2, 14, 19, and 22), the separation between the Commercial Reservoir and Connected Fracture Network is wider because this region is where other subsurface processes are ongoing, e.g., influx of marginal recharge, etc.

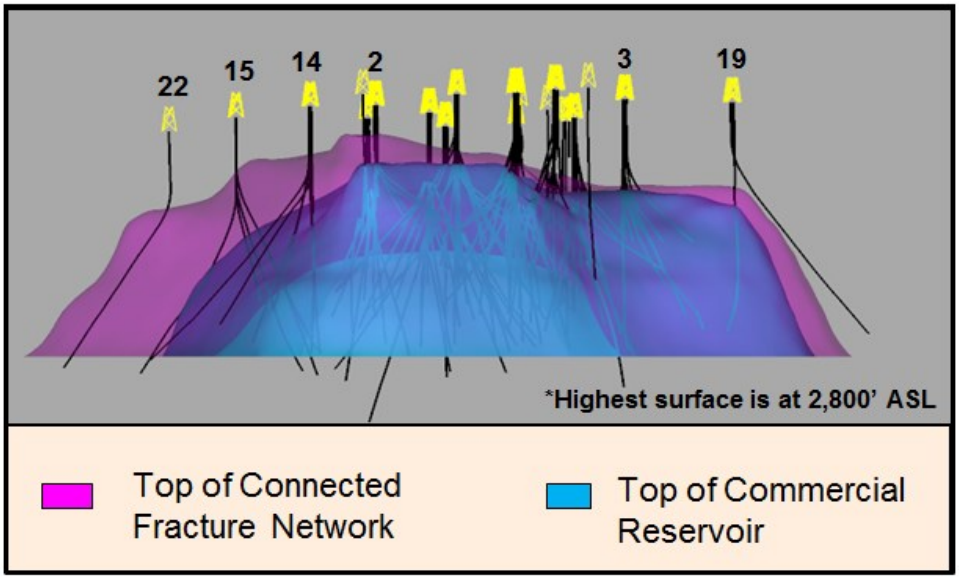

Figure 8: 3D model showing the Tops of Commercial Reservoir and Connected Fracture Network.

3.2 Base of Reservoir (BoR)

Similar with the ToR, the new terminologies used to define the BoR are the Base of Commercial Reservoir and Base of Connected Fracture Network. The criteria used to define the Base of Commercial Reservoir are similar with the criteria used to define the low case BoR in the previous Static Model (**Table 3**).

The criteria used to define the Base of Connected Fracture Network are a little bit more complicated. In the previous Static Model, the 0.5 MEQ density was the basis for the medium case BoR while 0.1 MEQ density was used to define the High Case. Although still using MEQ density, the main basis now is the MEQ events stimulated in the connected fracture system with injection activities. In areas where there are no injection-induced MEQs, the 0.5 MEQ density is still used to define the Base of Commercial Reservoir (**Table 3**).

Table 3: Criteria used to define Bases of Commercial Reservoir and Connected Fracture Network

Case	Criteria
Base of Commercial Reservoir	The deepest PTS entry encountered by deepest well in the pad plus 150 m.
Base of Connected Fracture Network	▪ Injection-induced MEQs that represent the connected fracture system stimulated by injection activity ▪ 0.5 MEQ density in areas without injection activity

Figure 9 shows the 3D model of the Bases of Commercial Reservoir and Connected Fracture Network. The depth of the MEQ events suggests that the connected fracture network could extend as deep as 12,600' BSL below well 9.

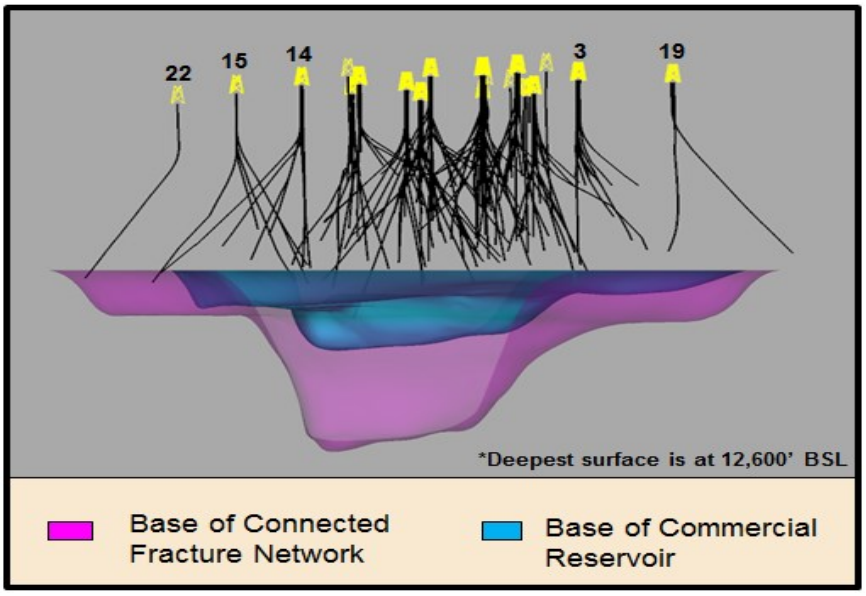

Figure 9: 3D model of base of commercial reservoir and base of connected fracture network.

3.3 GROSS ROCK VOLUME (GRV) COMPARISON

The Gross Rock Volume (GRV) was calculated and compared between the previous reservoir regions (i.e., Low and Mid cases) in the previous and the updated reservoir regions (i.e., Commercial Reservoir and Connected Fracture Network) in the current Static Model (**Figure 10**). There is a 4 km^3 (8.5%) difference in GRV in the previous compared with the current Static Model (**Table 4**). Meanwhile, the Connected Fracture Network is about 17 km^3 (43.5%) bigger than the Mid Case BoR in the previous Static Model. Although the GRV is bigger in the current 3D Static Model, it is believed that the definition of the reservoir regions aptly represents the current understanding of the conceptual model of a geothermal system.

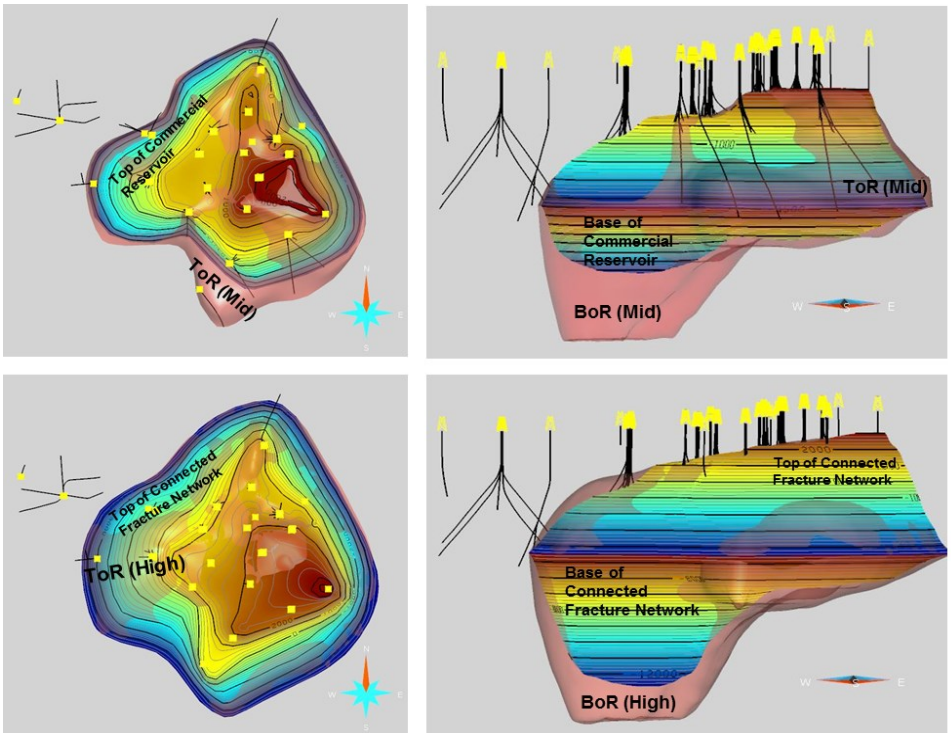

Figure 10: Comparison of reservoir surfaces between the previous and currrent (updated) 3D Static Models.

Table 4: GRV comparison between previous and current (updated) Salak 3D Static Model.

Previous Reservoir Region	GRV (km^3)	Current Reservoir Region	GRV (km^3)
Low Case	47	Commercial Reservoir	51
Mid Case	62	Connected Fracture Network	89
High Case	78		

4. MATRIX AND FRACTURE PROPERTY MODELING

4.1 Matrix Porosity and Permeability

The approach in distributing matrix porosity (Φ_{matrix}) and permeability (k_{matrix}) in the updated Salak 3D Static Model adapted the Best Practices from the Darajat 3D matrix property modeling. The distribution of matrix properties was based on each formation in the updated Salak stratigraphy grid. In the previous Static Model, matrix properties were populated using kriging method based on the 3D facies or Petrophysical Group (PG) distribution model.

The first step in updating the matrix property model was to calculate the average matrix property value for a certain PG in a certain formation. The PGs simplified the different lithologic units to a level that can be justified with reasonable confidence by considering the contrast mainly in the petrophysical properties, depositional styles, and hydrothermal alteration. From the nine different lithologies identified, five petrophysical groups were determined, namely, (1) marine sediments, (2) lava, (3) fine pyroclastics, (4) coarse pyroclastics, and (5) intrusion/skarn. The PG proportions in each formation that were used in averaging the matrix property values are summarized in **Table 5**.

Matrix property values for core samples inside the reservoir were used as representative porosity values; core samples from outside the reservoir were excluded. However, intrusion and skarn core samples from both inside and outside the reservoir were used due to the limited samples of these lithologies. Note that the intrusion and skarn matrix property values between inside (state the average value) and outside (state the average value) the commercial reservoir are not significantly different anyway. The total weighted Φ_{matrix} and k_{matrix} assigned in the 3D Static Model represents the average Φ_{matrix} and k_{matrix}, respectively, in each formation with certain PG proportions (**Figures 11** and **12**).

Table 5. PG proportion in each stratigraphic formation

Formation	Petrophysical Group				
	Marine Sediments	Lava	Fine Pyroclastics	Coarse Pyroclastics	Intrusion and Skarn
Upper Dacite	0%	35%	57%	8%	0%
Upper Andesite	0%	38%	42%	20%	0%
Middle Dacite	0%	22%	61%	17%	0%
Middle Andesite	0%	33%	43%	24%	0%
RDM	1%	18%	79%	2%	0%
Lower Andesite	1%	38%	50%	11%	0%
MSV	26%	21%	43%	10%	0%
Intrusion	0%	0%	0%	0%	100%

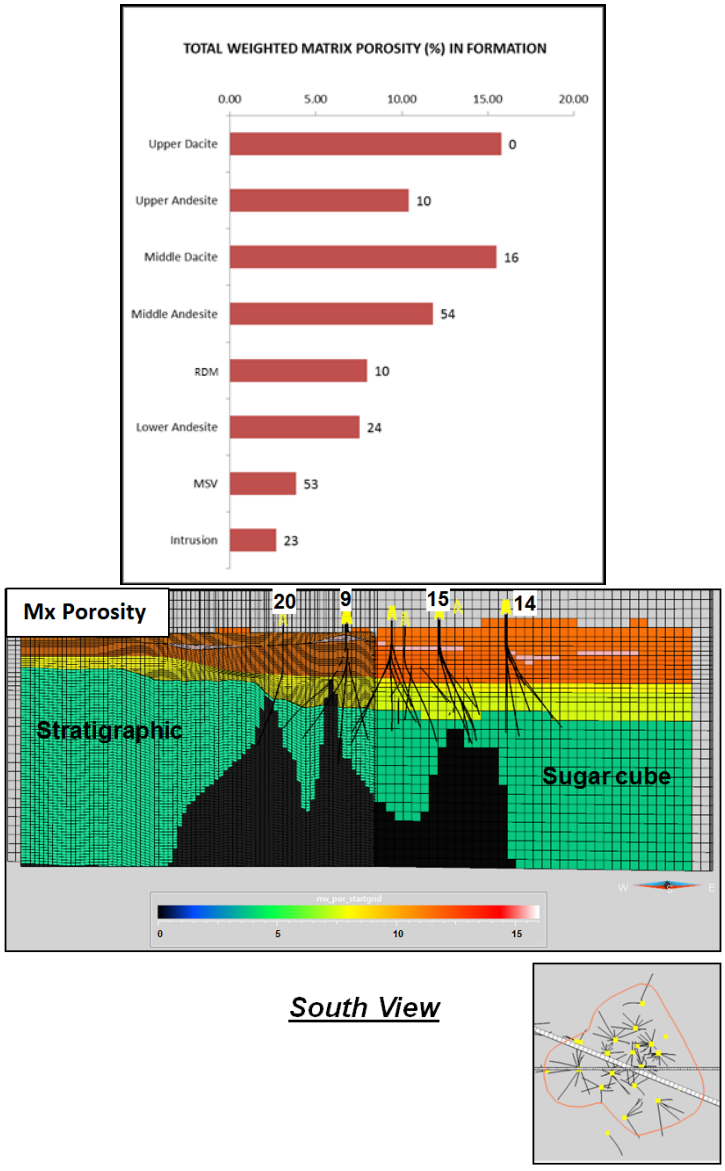

Figure 11: (Left) Chart showing the total weighted Φ_{matrix} in each formation assigned in the 3D Static Model. Values at the right side of the bar chart represent the number of core samples. There were no core samples in the Upper Dacite formation; thus, the Φ_{matrix} value in this formation used core samples from the Middle Dacite formation. Matrix porosity shows a discernible decreasing in trend with depth. (Right) 3D model of Φ_{matrix} showing its distribution in the stratigraphic grid of the previous Salak 3D Static Model (left side of the cross-section) and the resulting transfer into the sugar cube grid of the updated Salak 3D Static Model (right side of the cross-section).

4.2 Fracture Permeability ($k_{fracture}$) Modeling

The fracture permeability ($k_{fracture}$) model at Salak was developed using the Cumulative Average PI'[1] method. This method is a combination of the Modified Fractional PI' workflow and geostatistics to distribute $k_{fracture}$. The result from this approach is a 3D model of PI', which was then converted into the $k_{fracture}$ model using Background and Residual Models. The Background Model is an interpretation of the global trend in fracture permeability, and does not include all the details from well data (**Figure 13**). Meanwhile, the Residual Model incorporates the difference between the well data and the Background Model to honor the well data and discretize the $k_{fracture}$ model. The final $k_{fracture}$ model handed over to the Salak Numerical Modeling Engineers is a combination of both the Background and Residual Models. A residual weighting factor of 30% is applied to provide a good trade-off between limiting the "bulls'-eyes" and honoring well data (**Figure 14**). Also, this resulting model captures the general conceptual model of permeability in geothermal systems. Similar at Darajat (Golla et.al. 2015), $k_{fracture}$ decreases with depth exponentially at Salak. In terms of lateral distribution, high $k_{fracture}$ areas are found in the north and central

[1] PI' refers to the normalized Productivity Index (PI) without the effects of reservoir enthalpy and pressure (Acuna et.al. 2008).

portions of the Salak field. The average fracture permeability at Salak is about 96 mD in the connected fracture network and 116 mD inside the commercial reservoir.

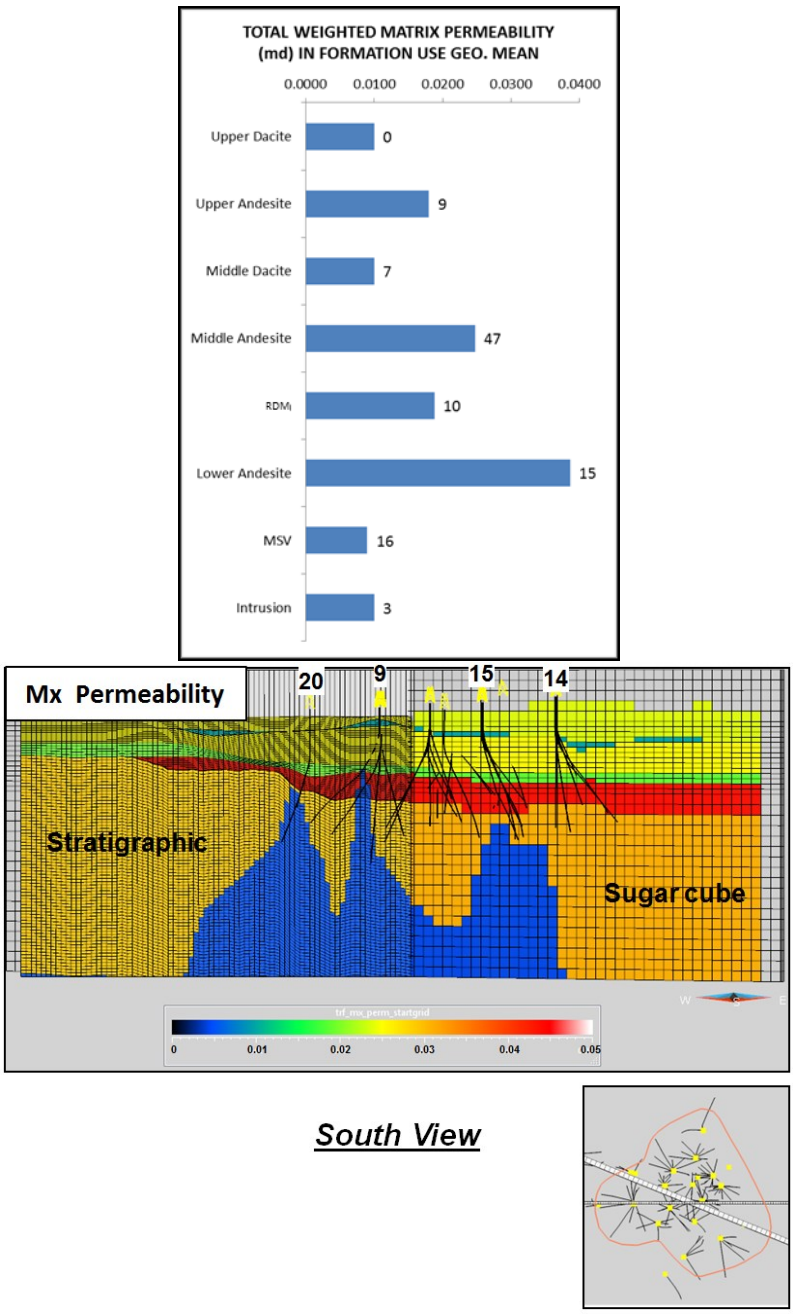

Figure 12: (Left) Chart showing the total weighted k_{matrix} using the geometric mean in each formation assigned in the 3D Static Model. Values at the right side of bar chart represent the number of core samples. There were no core samples in the Upper Dacite formation; thus, the k_{matrix} value in this formation used core samples from the Middle Dacite formation. Different with Φ_{matrix} trend, k_{matrix} does not show any discernible trend with depth. (Right) 3D model of k_{matrix} showing its distribution in the stratigraphic grid of the previous Salak 3D Static Model (left side of the cross-section) and the resulting transfer into the sugar cube grid of the updated Salak 3D Static Model (right side of the cross-section).

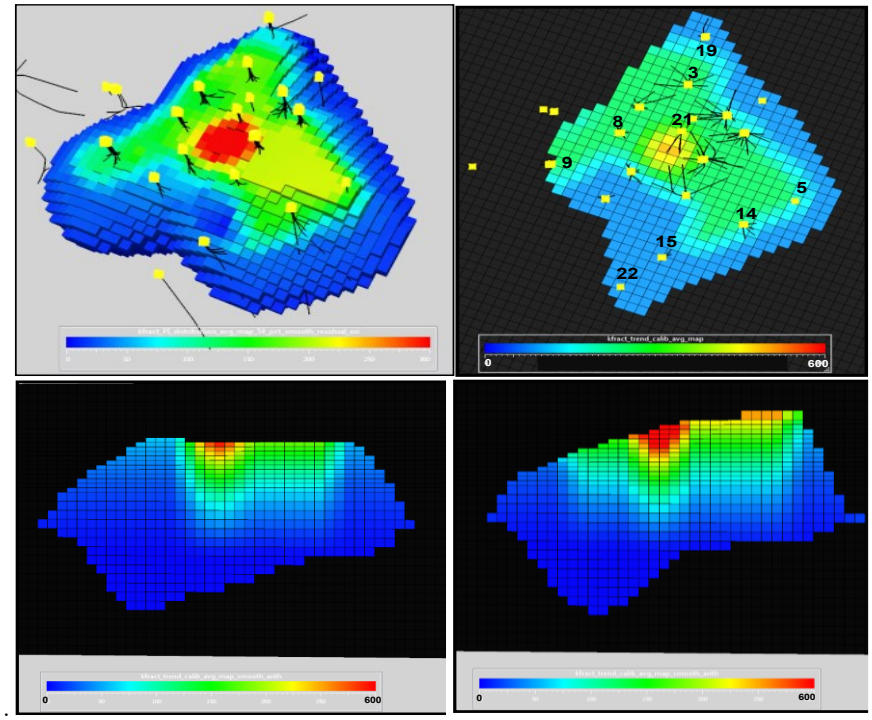

Figure 13: Background fracture permeability Model in the new oriented grid Showing the general trend across the Salak field.

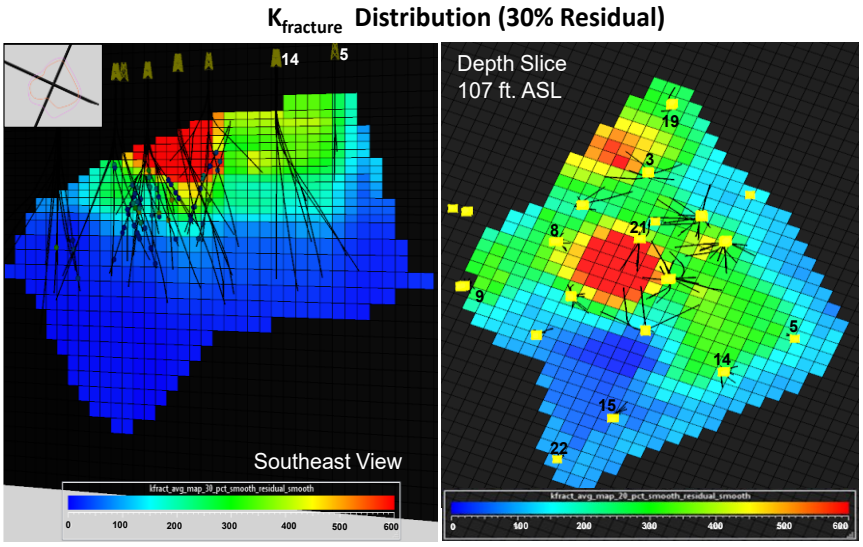

Figure 14: Fracture permeability distribution using 30% residual weighting. At this weighting, there is an acceptable trade-off between limiting the "bulls'-eyes" and maintaining high correlation coefficient. The average $k_{fracture}$ is 96 mD in the Connected Fracture Network region and 116 mD inside the commercial reservoir.

4.2 Fracture Spacing Modeling

The key data used in the fracture spacing analysis is the borehole image logs from where Fracture Density (i.e., 1/Fracture Spacing) is determined. However, the challenge is that the logged wells are relatively sparse. Hence, Fracture Frequency (FF) or the spacing of Effective Fractures (or feed zones) encountered during drilling was used to supplement the relatively sparse data set of wells with image logs. In the workflow, the patterns of the relatively well-constrained FF are used as a proxy to distribute the Fracture Density (FD), which is only available from wells with image logs.

To confirm that FF and FD trends are consistent, a comparison of average changes for both FF and FD trends vertically and aerially was conducted and summarized in **Figures 15** and **16**. Analyses show that both FF and FD decrease with depth while EF Spacing decreases from the south towards north Salak. These trends were then represented in the 3D Static Model.

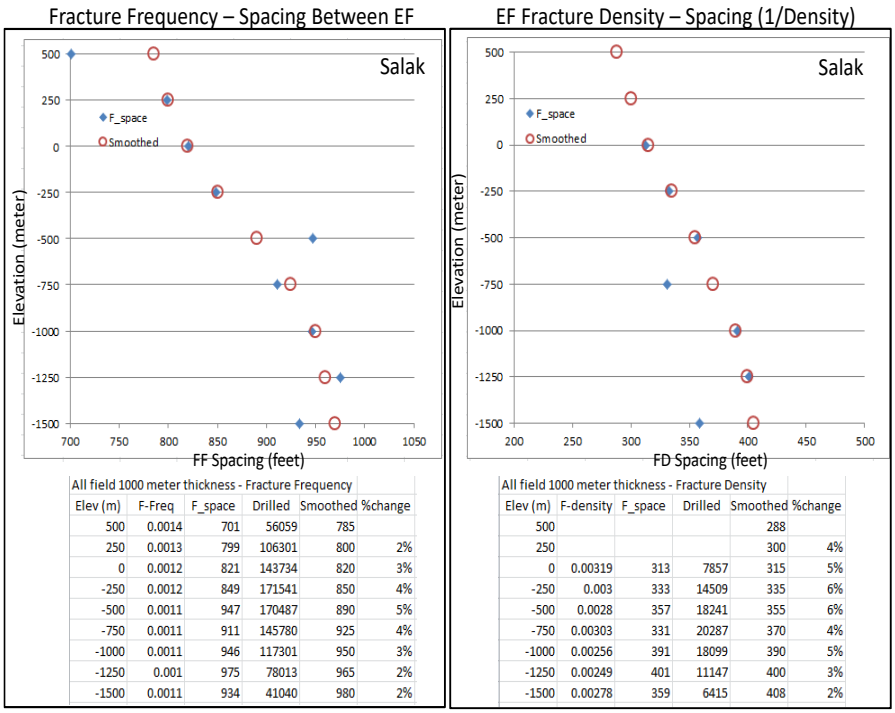

All field 1000 meter thickness - Fracture Frequency

Elev (m)	F-Freq	F_space	Drilled	Smoothed	%change
500	0.0014	701	56059	785	
250	0.0013	799	106301	800	2%
0	0.0012	821	143734	820	3%
-250	0.0012	849	171541	850	4%
-500	0.0011	947	170487	890	5%
-750	0.0011	911	145780	925	4%
-1000	0.0011	946	117301	950	3%
-1250	0.001	975	78013	965	2%
-1500	0.0011	934	41040	980	2%

All field 1000 meter thickness - Fracture Density

Elev (m)	F-density	F_space	Drilled	Smoothed	%change
500				288	
250				300	4%
0	0.00319	313	7857	315	5%
-250	0.003	333	14509	335	6%
-500	0.0028	357	18241	355	6%
-750	0.00303	331	20287	370	4%
-1000	0.00256	391	18099	390	5%
-1250	0.00249	401	11147	400	3%
-1500	0.00278	359	6415	408	2%

Figure 15: Charts showing FF and EF Density trends with depth at Salak. The EFs used for FF are the fractures that have been clearly identified from PTS surveys that contribute to wellbore flow.

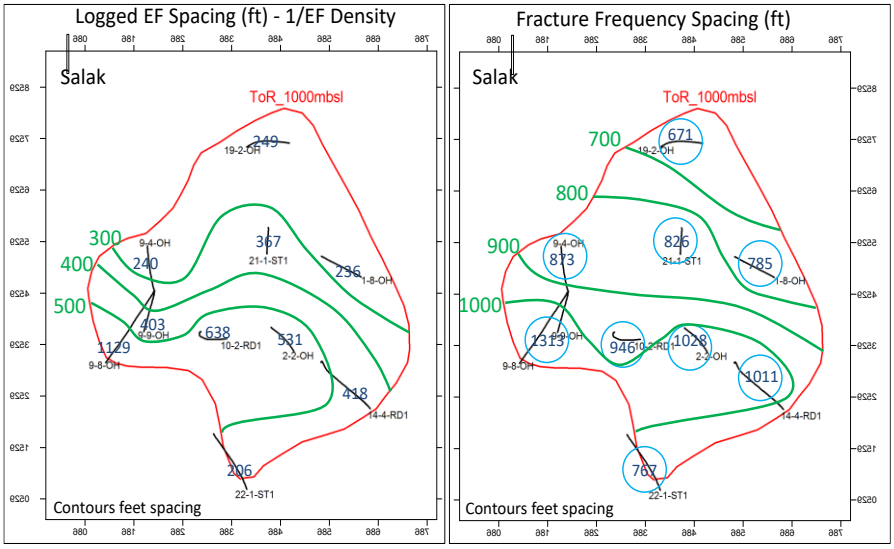

Figure 16: Maps showing the aerial distribution of FF and EF Density at Salak. The well courses shown are those with borehole image logs only. For FF, all the wells within a binned area (blue circle) were used to estimate the average spacing.

Figure 17 shows the results of the distribution of Fracture Spacing at Salak aerially and along NW-SE and SW-NE cross-sections. Note the similarity in both vertical and lateral distribution of Fracture Spacing in **Figure 17** with the trends shown in **Figures 15** and **16**.

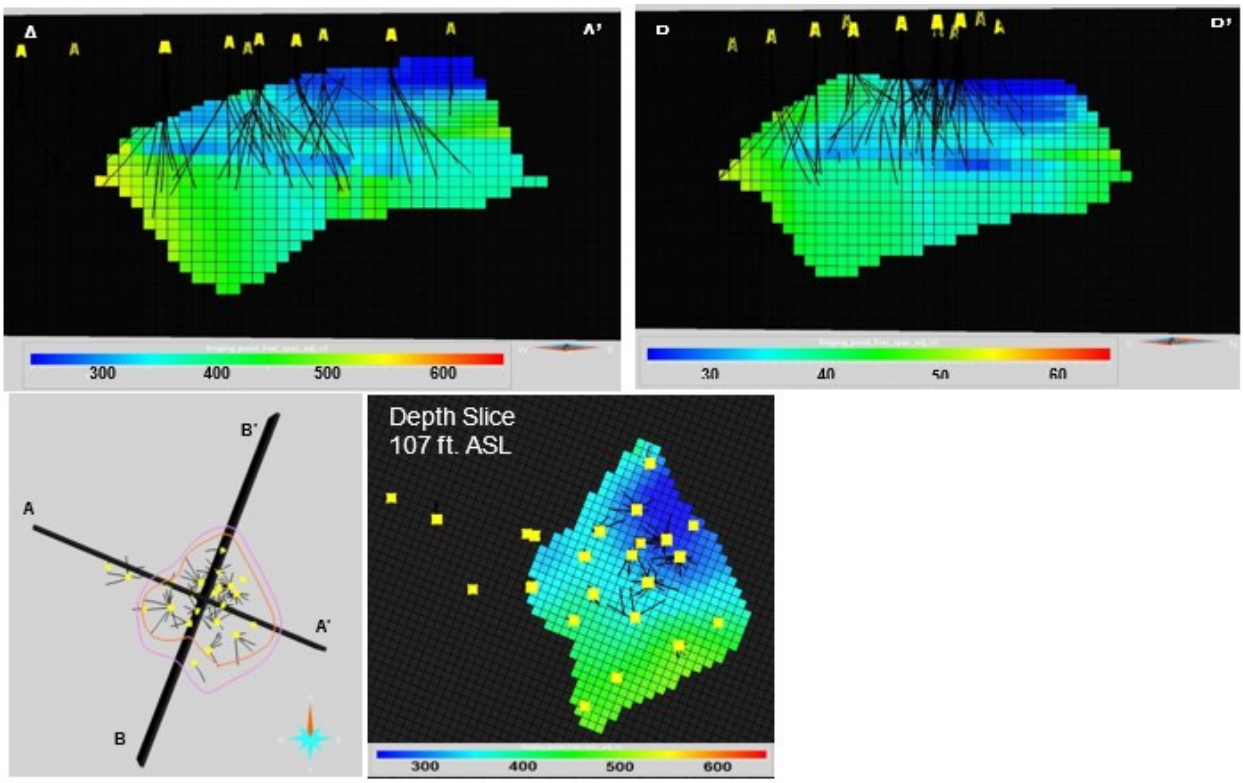

Figure 17: 3D Fracture Spacing model using the patterns and distribution of FF as a proxy. Extrapolation was conducted especially in areas with no well data.

5. SUMMARY

The updated Salak 3D Static Model included the application of Best Practices for interpretation and distribution of Φ_{matrix} and k_{matrix} and new insights that have resulted from a fracture characterization study. The Salak 3D Static Model can now provide 3D distributions of $k_{fracture}$ and fracture spacing that are data-driven and conceptually reasonable. A Numerical Model is not unique and many potential representations of these parameters are possible each of which can provide an adequate basis for a history match. By providing "real earth" constraints for these parameters, the numerical representation of the geothermal reservoir will more accurately represent the subsurface condition and should result in improved and more credible estimates of future field performance. Additionally, it is expected that, with improved constraints, the initial "estimate" will be closer to the real earth case. Having the reservoir and fracture properties built in the 3D Static Model and, later, the Numerical Model should save the Numerical Modeler some time when fine-tuning these properties during the tedious history matching.

REFERENCES

Acuna, J., Sirad-Azwar, L., Pasikki, R., and Stimac, J.: Reservoir management at Awibengkok geothermal field, West Java, Indonesia, *Geothermics*, **37** (2008), pp. 332-346.

Aprilina, N.V., Satya, D.Y., and Golla, G.: Geologic Modeling Workflow for Volcanic Hosted Geothermal Reservoirs: Case Study from Salak Geothermal Field, *Proceedings*, World Geothermal Congress (2015).

Aprilina, N.V., and Putra, F.J.: Salak 3D Model Update Documentation, *Unpublished Star Energy Geothermal presentation file* (2016),.

Fitriyanto, A., Intani, R.G., Mahagyo, P., Golla, G., and Waite, M.: The 2012 Darajat 3D Static Model: General Workflows and Steps to Build a 3D Static Model, *Unpublished Star Energy Geothermal Report* (2012).

Golla, G., Intani, R.G., Pamurty, N.P., Putra, F.J., Satya, D.Y., and Gunderson, R.: Characterization of Permeable Entries and Fractures at the Salak, and Darajat Geothermal Reservoirs, *Unpublished Star Energy Geothermal Report* (2015).

Nordquist, G.: Fracture Spacing Distribution in Earth Models Salak and Darajat, *Unpublished Star Energy Geothermal Report* (2017).

Satya, D.Y., Putra, F.J., and Golla, G., Fracture Permeability Modeling: Approach and Current Method at Darajat and Salak, Naturally Fractured Reservoir (NFR) Project Report, *Unpublished Star Energy Geothermal Report* (2017).

Stimac, J., Nordquist, G., Suminar, A. and Sirad-Azwar, L.: An Overview of the Awibengkok Geothermal System, Indonesia, *Geothermics*, **37** (2008), pp. 300-331.